Proceedings of the ASME 2020
Internal Combustion Engine Division Fall Technical Conference
ICEF2020
November 1-4, 2020, Denver, CO, USA

ICEF2020-2992

MULTI-DIMENSIONAL MODELING OF THE CFR ENGINE FOR THE INVESTIGATION OF SI NATURAL GAS COMBUSTION AND CONTROLLED END-GAS AUTOIGNITION

Diego Bestel, Scott Bayliff, Anthony Marchese, Daniel Olsen, Bret Windom.[1]
Colorado State University
Fort Collins, CO

Hui Xu
Cummins Inc.
Columbus, IN

ABSTRACT

Engine knock and misfire are barriers to pathways leading to high-efficiency Spark-Ignited (SI) Natural Gas engines. The general tendency to knock is highly dependent on engine operating conditions and the fuel reactivity. The problem is further complicated by low emission limits and the wide range of chemical reactivity in pipeline quality natural gas. Depending on the region and the source of the natural gas, its reactivity, described by its methane number (analogous to the octane number for liquid SI fuels) can span from 65 - 95. In order to realize diesel-like efficiencies, SI natural gas engines must be designed to operate at high BMEP near knock limits over a wide range of fuel reactivity. This requires a deep understanding regarding the combustion-engine interactions pertaining to flame propagation and end-gas autoignition (EGAI). However, EGAI, if controlled, provides an opportunity to increase SI natural gas engine efficiency by increasing combustion rate and the total burned fuel, mitigating the effects of the slow flame speeds of natural gas fuels which generally reduce BMEP and increase unburned hydrocarbon emissions. For this reason, in order to study EGAI phenomenon, the present work highlights multi-dimensional computational fluid dynamics (CFD) models of the Cooperative Fuel Research (CFR) engine. The CFR engine models are used to investigate fuel-engine interactions that lead to EGAI with natural gas, including effects of fuel reactivity, engine operating parameters, and exhaust gas recirculation (EGR). A Three-Pressure Analysis, performed with GT-Power, was used to estimate initial and boundary conditions for the three-dimensional CFD model. CONVERGE CFD v2.4 was used for the three-dimensional CFD modeling where the level set G-Equation model and SAGE detailed chemical kinetics solver were used. An assessment of the different modeling approaches is also provided to evaluate their limitations, advantages and disadvantages, and for which situations they are most applicable. Model validation was performed with experimental data taken with a CFR engine over varying compression ratio, CA50, EGR fraction, and IMEP and shows good agreement in Peak Cylinder Pressure (PCP), PCP crank angle, and the location of the 10%, 50%, and 90% mass fraction burned (CA10, CA50, and CA90, respectively). The models can predict the onset crank angle and pressure rise rate for light, medium, and heavy EGAI under a variety of fuel reactivities and engine operating conditions.

1. INTRODUCTION

With increasing concern regarding green-house gases (GHG) emission and air pollution, environmental regulations have become stricter when it comes to emissions from internal combustion (IC) engines. According to [1], [2] the world's transportation fleet will be primarily powered by IC engines in the foreseeable future and will account for around ~40% of energy demand by 2040 [3]. Additionally, the transport sector is expected to increase ~75%, with diesel fuel demand increasing by 85% [2]. For this reason, the study of alternative and cleaner fuels is necessary to address issues such as global warming and human health problems caused by air pollution from tailpipe emissions.

Natural gas (NG) is a compelling substitute for diesel fuel in the medium and heavy-duty market since it offers advantages such as reduced emissions and fuel costs. Currently in the U.S., the cost of diesel fuel on an equivalent energy basis is approximately five times the cost of NG [4]. Additionally, lower capital and operating costs, vast availability of NG domestically, lower particulate matter (PM) emissions, lower CO_2 emissions, and simpler and inexpensive aftertreatment system offer further advantages for using NG over diesel. However, NG engines are

[1] Contact author: Bret.Windom@colostate.edu

typically less efficient than diesel engines, have less energy density, and have limited refueling infrastructure, reasons that have prevented the use of NG engines in the medium and heavy-duty markets. Therefore, increasing NG engine efficiency is necessary to address these issues and accelerate NG engine market penetration.

Spark-ignited (SI) NG engine efficiency can be enhanced by: (1) increasing compression ratio (CR) and or boost pressure, (2) increasing charge density through the use of cooled Exhaust Gas Recirculation (EGR), and (3) enhancing the rate of combustion. Improvements in any of these parameters are challenging since they are limited by knock, misfire, and emissions. Knock, the auto-ignition of the unburned mixture ahead of the main propagating flame front, limits the improvements on efficiency since its occurrence is highly dependent on fuel reactivity/quality and engine operating conditions. It is known that advanced spark timings, higher CR, and boosted pressures increase engine efficiency [5], however, they also increase the tendency to knock and their tuning is limited in order to avoid unstable knocking combustion events [6]. Knocking combustion not only decreases engine efficiency but can also cause severe damage to the engine.

A measure of the fuel reactivity quality and its tendency to knock is the Methane Number (MN), which is a scale ranging from 0 to 100 where 0 represents the most reactive mixture, equivalent to a mixture of 100% H_2, and 100 represents the least reactive mixture, equivalent to a mixture of 100% CH_4. Similar to the Octane Number for gasoline blends, the MN of a fuel blend will be defined by that of having equal knocking behavior of a H_2 and CH_4 mixture. The MN has high variability in the US which adds an additional difficulty to increasing SI NG engine efficiency. Currently, NG SI engines are designed for the worst-case fuel quality, lowest MN, resulting in suboptimal performance for the average fuel reactivity.

Fundamental research is needed to better understand the underlying combustion phenomena to enable optimization of the engine design parameters and develop control algorithms to expand knock, misfire, and emission limits**.** For this reason, the present work highlights multi-dimensional computational fluid dynamics (CFD) models of the Cooperative Fuel Research (CFR) engine in order to study the fuel-engine interactions that lead to End-Gas Autoignition (EGAI). Models capable of accurately predicting EGAI can be used to develop strategies on how to control EGAI and accounting for varying fuel reactivity, engine operating parameters, and exhaust gas recirculation (EGR).

2. ENGINE DETAIL AND OPERATING CONDITIONS

The standardized Cooperative Fuel Research (CFR) F1/F2 engine available at the Engines and Energy Conversion Laboratory (EECL) at Colorado State University (CSU) was used to carry out the necessary experiments to validate CFD models. The CFR engine is a single-cylinder, four stroke, SI engine with a two-valve head. The engine has a stroke of 114.3 mm (4.5 in.) and a bore of 82.55 mm (3.25 in.). The design of the cylinder/head assembly allows the CR to be varied from 4:1 to 18:1 during engine operation. The CFR engine is a useful tool for validating knock models because it is designed to withstand repeated knocking events. Thus, it can be operated at varying knock levels and compared with simulation results for the same operating conditions. Originally designed to measure the research octane number (RON) of liquid fuels [7], the engine has been converted to operate on gaseous fuels for the study of combustion properties and measurement of methane number (MN). The test cell is equipped with a fuel blending system designed to test gaseous fuels with up to 8 components. The system incorporates intake air and exhaust back pressure control, which permits testing while simulating boosted conditions.

During the experiments crank angle resolved combustion pressure is measured using a flush mounted water-cooled, piezoelectric transducer Kistler model 6061A and intake and exhaust crank angle resolved pressures are measured using Kistler dynamic pressure sensors model 4007D and 4049B, respectively. Additionally, time-averaged intake and exhaust temperatures are measured using type K thermocouples. More detailed information on the CSU's CFR engine can be found in [8], [9], [10], [11].

For this work, a total of 51 operating points were tested to acquire the necessary data needed to support model development. The test points swept combustion phasing marked by the location at which 50% of fuel energy is released (CA50: 6.7-31.9 deg. aTDC), break mean effective pressure (BMEP: 3.2-7.0 bar), EGR levels (0-20%), and CR (7.41-14.1:1). Additionally, three different fuel compositions were tested under the Methane Number (MN) test procedures as detailed in Wise et al. [12]. This strategy made it possible to observe four knock regimes: non-knocking, light knock, medium knock, and heavy knock. Table 1 shows the compositions and experimentally determined MN of the four tested fuels. The Pipeline 1 and 2 fuels were sourced from the NG pipeline supplying the lab on two separate days of testing. The dry fuel composition was custom blended and selected to represent a typical high MN NG supply and the Wet blend was formulated to mimic the composition of a reactive natural gas. The Pipeline 2, Dry, and Wet fuels were tested under MN test conditions and as such data with their H_2/CH_4 reference mixtures were also acquired.

	Mol %			
Species	**Pipeline 1**	**Pipeline 2**	**Dry**	**Wet**
CH_4	84.5%	82.4%	97.04%	84.0%
C_2H_6	10.8%	12.5%	2.80%	13.3%
C_3H_8	1.4%	1.9%	0.04%	2.5%
C_4H_{10}	0.5%	0.5%	0.01%	0.1%
C_5H_{12}	0.2%	0.1%	0.00%	0.0%
C_6H_{14}	0.1%	0.0%	0.00%	0.0%
N_2	0.6%	0.4%	0.11%	0.1%
CO_2	1.9%	2.3%	0.00%	0.0%
MN	69	72.9	87.2	69.2

Table 1: Natural Gas compositions tested on the CFR engine.

3. COMPUTATIONAL MODELS

Multi-dimensional computational fluid dynamics (CFD) models of the CFR engine were created to investigate fuel-

engine interactions that lead to EGAI with natural gas to gain insight on the parameters which could allow one to control its occurrence. Multiple modeling approaches were performed and their suitability for the various analysis strategies were evaluated. This section describes details of the three modeling approaches used. All models presented in this work were based on the solid CFR engine models generated using an X-Ray scan by Argonne National Laboratory [13], [14] with minor changes highlighted in section 3.2.

3.1 1-D Three Pressure Analysis Model

A 1-D Three-Pressure Analysis (TPA) CFR model was created using GT-Power [15]. The outputs of this model were later used to define initial and boundary conditions for subsequent CFD engine modeling, as discussed later. The 1-D TPA GT-Power modeling approach is a non-predictive analysis performed to calculate parameters that are difficult or impossible to be measured in the test cell such as burn rate, wall temperatures, trapping ratio, residual fraction, etc. Three crank angle resolved pressures are necessary as inputs: intake, exhaust, and cylinder pressure together with time-averaged intake and exhaust temperatures. To correctly account for the volumetric efficiency, discharge coefficients were used according to [16] and valve lift profiles at zero valve lash according to [13]. Cylinder walls, ports, and valve temperatures were calculated using the Cylinder Wall Temperature Solver and the Finite Element Cylinder Structure Geometry modules on GT-Power, employing the Woschni correlation [17]. With this simplified 1-D model, initial and boundary conditions, e.g. wall temperatures, in-cylinder temperature, and intake and exhaust initial gas temperatures were calculated and used in the 3-D CFD models. Additionally, the 1-D model provides the amount of expected Residual Gas Fraction (RGF) necessary for the generation of the laminar flame speed tables that will be discussed later. Figure 1 shows the TPA model of the CFR engine.

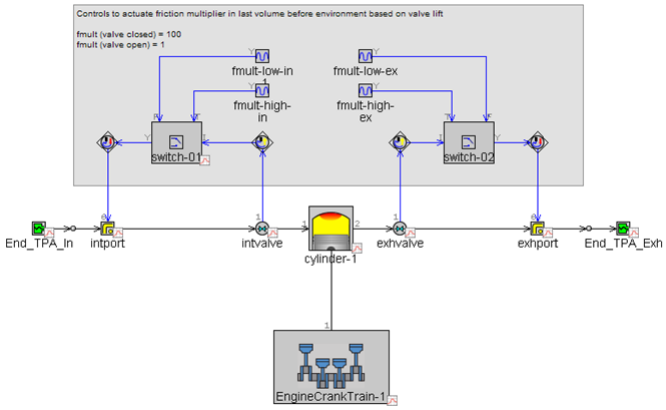

Figure 1: 1-D TPA GT-Power model.

3.2 3-D CFD Model with Chemical Kinetics

CONVERGE CFD version 2.4 [18] was chosen to carry out the 3-D modeling in this work. CONVERGE CFD offers very practical solutions for mesh manipulation such as automatic mesh generation during runtime, fixed embedding, which refines the mesh in specified locations at specified times set by the user, and Adaptive Mesh Refinement (AMR), which refines the mesh automatically based on parameters set by the user. These features make it a robust tool for the full-cycle simulation of engines, being capable of optimizing the mesh for better accuracy while not penalizing on simulation time.

As mentioned previously, the surface mesh was generated from an X-ray scan performed by Argonne National Laboratory and incorporates realistic geometry features of the intake and exhaust ports, knockmeter cavity, spark plug, and the 180º intake valve shroud. Figure 2 shows the surface of the CFR engine used in the 3-D simulations. This surface mesh was updated from the original (Argonne's engine) to better match the conditions found in the CSU-CFR engine. Namely, the knockmeter cavity, spark plug, and piston crevice were updated and/or added to account for the actual geometry of the CFR engine at CSU. The pressure transducer for the in-cylinder pressure measurement is installed on the knockmeter cavity and is flush with the cylinder head. The actual spark plug used in the engine testing was measured and its dimensions were included in the model to account for the correct spark plug gap, J plug, crevice volume dimensions, and orientation.

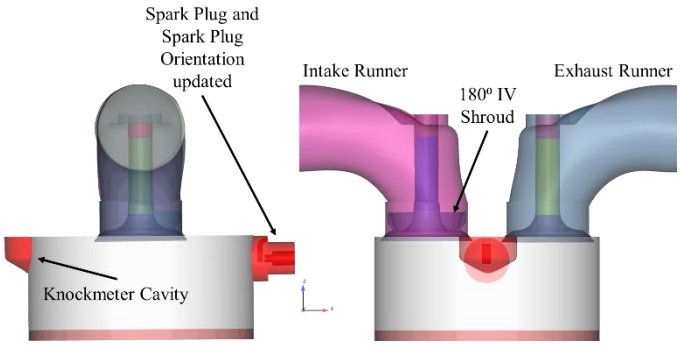

Figure 2: CFR Surface used in the 3-D CFD simulations. Features in red were updated.

The base grid size for the mesh generation used in this study was 4 mm outside of the cylinder. Inside the cylinder a permanent fixed embedding for the cylinder region was used to refine the base grid down to 1 mm. Four levels of fixed embedding were specified to compute the spark kernel and initial flame propagation (grid size of 0.250 mm). Near the walls, three levels of boundary embedding were added to resolve heat transfer. Additionally, AMR was used to refine grid size down to 0.5 mm inside the cylinder based on temperature and velocity subgrid scales of 2.5 K and 1 m/s, respectively. Turbulence was modeled with the Reynolds-Averaged Navier-Stokes (RANS) and re-normalized group (RNG) k-ε model. According to [19], [20], [21] the grid sizes chosen are sufficient to simulate normal and knocking combustion with RANS in SI engines. To account for wall heat transfer, the model proposed by O'Rourke and Amsden [22] was employed.

Two combustion modelling approaches were used in this work to model flame propagation and EGAI: (1) exclusively SAGE, a chemical kinetics solver, and (2) a coupled G-Equation

(to solve flame propagation) with SAGE (to solve the chemistry in the burned and unburned gas) approach. The latter will be called G-Equation in the remainder of this paper for simplicity.

SAGE is a chemical kinetics solver which uses detailed chemistry to track combustion in the domain and its full description can be found in [18] and [23]. To initiate combustion, a model for the spark event is necessary. In order to model the spark appropriately, two spherical energy sources of 0.5 mm in radius were used in the spark plug gap between the electrodes, creating a "L" energy deposit profile which represents the breakdown, arc and glow phases. The durations of each energy deposition event were 0.5 degrees for the first event and up to 16 degrees for the second. Their intensities were selected based on the parameters measured during CFR engine testing, i.e. up to 125 mJ. The chemical mechanism used in this work for all models is a reduced mechanism from ARAMCO 3.0 [24] with 82 species and 519 reactions, named ARIES82 [25], [26]. Below, Figure 3 compares calculated ignition delays for ARAMCO 3.0 and ARIES82 at 40 bar and stoichiometry.

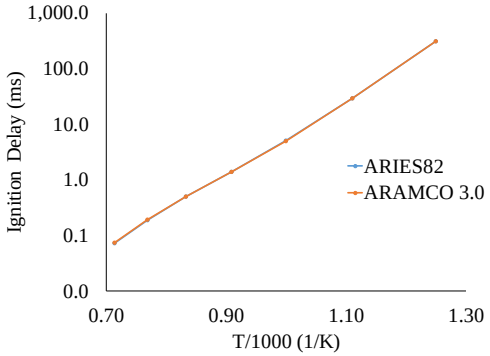

Figure 3: Ignition delay comparison between ARAMCO 3.0 and ARIES82 for the Pipeline 2 NG composition. No EGR was used in this case.

3.3 3-D CFD Model with Level Set Approach

The G-Equation Flamelet Model based on the Level Set Approach [27] was also used to simulate the CFR engine. In this model, the turbulent premixed combustion is assumed to occur in either the corrugated or thin reaction zone regimes and, therefore, the turbulent flame can be tracked by solving a transport equation for the non-reacting scalar G [28],

$$\frac{\partial \rho \tilde{G}}{\partial t} + \frac{\rho \widetilde{u_i} \tilde{G}}{\partial x_i} = -\rho D_t \tilde{\kappa} \left|\frac{\partial \tilde{G}}{\partial x_i}\right| + \rho_u s_t \left|\frac{\partial \tilde{G}}{\partial x_i}\right| \quad (1)$$

where ρ and ρ_u are the burned and unburned density, D_t the turbulent diffusivity, $\tilde{\kappa}$ the mean flame front curvature, and s_t the turbulent flame speed. As it can be seen in equation (1), the turbulent flame speed s_t is required in order to track the flame propagation using the G-Equation, which is calculated for RANS turbulence models using [27]

$$s_t = s_l + u' \left\{ -\frac{a_4 b_3^2}{2b_1} Da + \left[\left(\frac{a_4 b_3^2}{2b_1} Da \right)^2 + a_4 b_3^2 Da \right]^{1/2} \right\} \quad (2)$$

where s_l is the laminar flame speed and b_1, b_3, and a_4 are modeling constants. Since s_l is an input to the model, ARAMCO 3.0 and the 1-D chemistry tool in CONVERGE CFD were used to calculate s_l for each fuel and generate a lookup table before any CFD simulation was run. The range of parameters used to generate the flame speed lookup tables were 400-1100 K for temperature with 100 K steps, 10-70 bar for pressure with 5 bar steps, 0.7-1.3 for equivalence ratios with 0.1 steps, and 0-30% of dilutants with 10% steps. The maximum concentration of dilutants was chosen to be 30% by mass since the sum of the RGF plus EGR did not exceed 30% in the experiments as estimated using the 1-D TPA model. In this work, the calibration process found that b_1 equal to 2.1 is sufficient to simulate all cases.

4. RESULTS

4.1 1-D TPA Model

Model validation was performed using data acquired for Pipeline 1 NG at a variety of CA50, BMEP, and EGR rates. In order to ensure proper volumetric efficiency and, therefore, correct trapped mass for each operating condition, intake valve flow area multiplier was set to 1.25 for all cases, which ensured fuel flow rates and air flow rates agreed within 5% of the measurements, which is within the measurement uncertainty. Correctly matching fuel energy at each operating point makes the tuning of the overall cylinder heat transfer convection multiplier reasonable since heat transfer is modeled using correlations that might not be accurate during knocking combustion [13]. Therefore, the overall cylinder heat transfer multiplier was varied up to 1.15 to match net IMEP. Gamma Technologies recommends a maximum of 1.1 [15], however, other research have successfully used multipliers up to 3 [13]. Figure 4 shows predicted versus measured fuel and air flow rate for all test conditions.

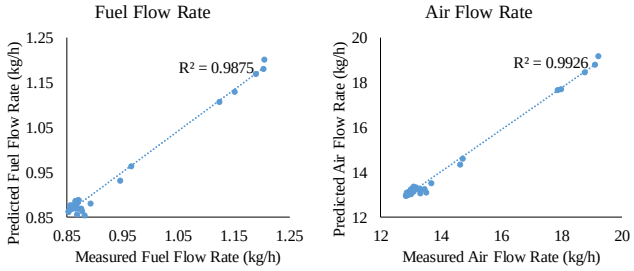

Figure 4: Predicted vs measured fuel and air flow rates.

Performance parameters also agree well with all test cases matching experimental CA50 within 2 deg. and all but two cases within 1 deg. Average Peak Cylinder Pressure (PCP) is also within 2%, and PCP location within 1 deg. Figure 5 shows plots of the predicted versus measured quantities mentioned above. Figure 6 shows two representative cylinder pressure traces.

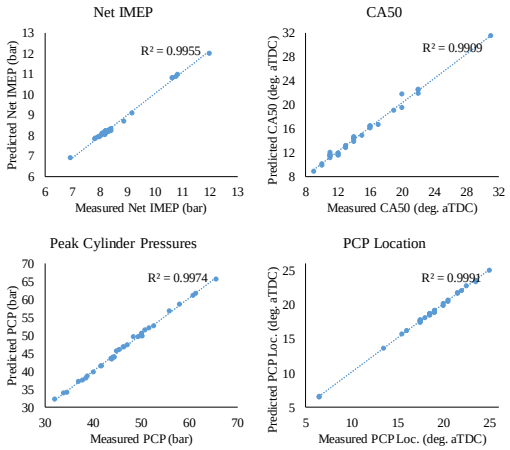

Figure 5: Net IMEP, CA50, PCP, and PCP location. Comparison of predicted vs measured.

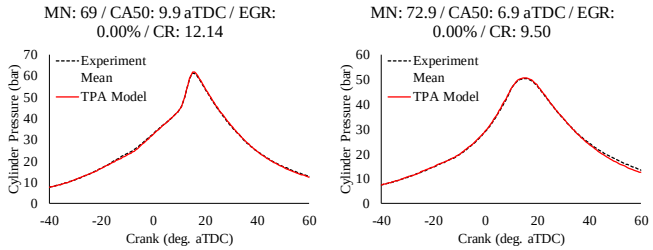

Figure 6: Cylinder pressure traces from GT-Power TPA model.

4.2 3-D CFD Models

Ten operating points were simulated using the 3-D CFD models for four different fuel compositions: Pipeline 1, Pipeline 2, the Reference H_2/CH_4 MN blend for Pipeline 2, and the Dry NG. Simulations with Pipeline 1 had parameters such as CA50, CR, BMEP, and EGR varied to achieve different operating conditions and knock intensities (KI) calculated according to procedure in Wise et al. [12]. For Pipeline 2, the MN Reference H_2/CH_4 blend, and the Dry NG, tests were carried out under the MN test procedure conditions, as reported in [10], therefore, spark timing for these cases was held constant. This differed from the tests with Pipeline 1 where the spark timing was allowed to vary to maintain constant CA50 from cycle to cycle.

Since the KI for operating conditions under the MN test are low and spark timing is fixed, the Pipeline 2 cases and the corresponding MN Reference blend were selected for the G-Equation Level Set Approach model calibration. If the model is tuned to predict burn rates and light knocking events just beyond the knock limit of such different fuel compositions, as required by the MN test procedure, it will be able to predict the onset of stronger knocking events when higher end-gas temperatures (from higher BMEP) are present. This is due to the exponential decrease in ignition delays and their reduced uncertainty at higher temperatures. This model calibration process found that b_1, a model constant used in equation (2), equal to 2.1 is sufficient. All ten simulated operating points were run for one engine cycle with initial and boundary conditions estimated using the 1-D TPA model. Table 2 shows the range of the wall temperatures used in the CFD simulations. Additionally, a lower spark energy, 20mJ, was sufficient to achieve stable combustion and satisfactorily match CA10 in the G-Equation model.

Boundary	Temperature (K) Min	Max
Cylinder Wall	425.76	463.38
Cylinder Head	456.45	539.93
Piston	422.49	459.04
Int. Valve Face	483.96	605.15
Exh. Valve Face	522.72	670.93
Int. Valve Rod	428.86	490.75
Exh. Valve Rod	462.27	544.63

Table 2: Wall temperature range used in the CFD simulations. Temperatures were estimated using the 1-D TPA model.

SAGE model calibration started from the calibrated G-Equation model. It was found that SAGE is more sensitive to spark energy. A spark energy of 20mJ was not enough to achieve good CA10, CA50, and PCP agreement and, therefore, was increased to 125mJ, closely matching energies used in experiments. Additionally, a large sphere embedding around the spark plug was necessary to properly match CA10 and CA50. Figure 7 shows a comparison of the spark settings on the heat release rate plot.

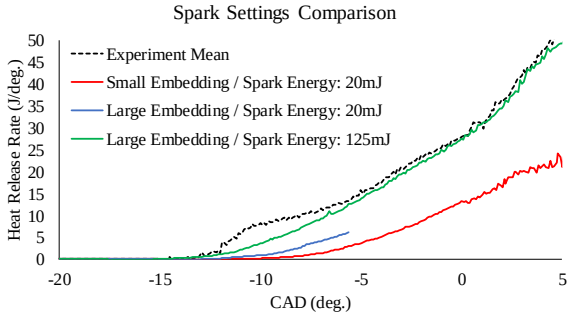

Figure 7: Spark settings comparison where not successful simulations were stopped to save computational time.

Figure 8 shows CFD results for three different cases (from top to bottom): light knock used in the G-Equation calibration, medium knock with SAGE, and heavy knock with G-Equation approach. As it can be seen, good agreement in cylinder pressure trace and heat release rate is found for all cases. In fact, average error for PCP is -0.03%, PCP location: +1.01 deg., CA50: +0.12, and IMEP: +2.4%. For the knocking cases, knock onset crank angle (KOCA) was predicted on average 1.65 degrees later than the experiments, resulting in an average of 3.5% lower fractional EGAI (f-EGAI), which is the fraction of the total energy released by the end-gas autoignition event. The reason for this later knock event is perhaps due to the uncertainties in the reduced

mechanism and the fact that NOx (present in the EGR) chemistry was not accounted for here, but has been shown to shorten ignition delay times as suggested by [25], [26], [29], [30].

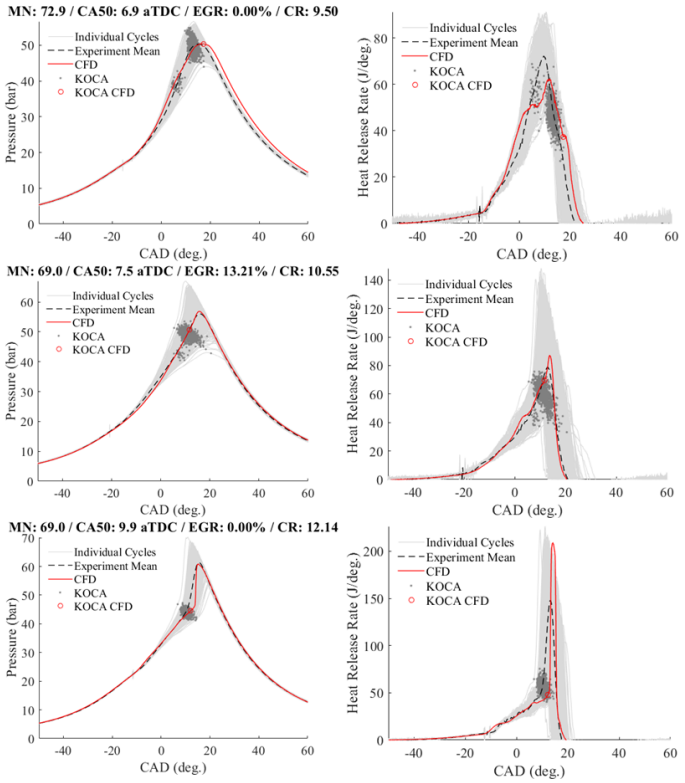

Figure 8: Top: Pipeline 2 model calibration result, MN rating test conditions (shown in Figure 6). Middle: SAGE result for Pipeline 1 with CA50 at 7.5 deg. aTDC and CR 10.55. Bottom: G-Equation result for Pipeline 1 with CA50 at 9.9 deg. aTDC and CR 12.14 (shown in Figure 6).

5. DISCUSSION

5.1 Models Comparison

Having calibrated the three different computational models for the CFR engine, a comparison of the models is presented, detailing what the authors found as advantages and disadvantages of each approach.

The 1-D TPA model is a non-predictive model where experimental data is required. Using experimental data, GT-Power calculates the burn rate for each operating point in an iterative manner. From the calculated burn rate, other parameters are then calculated resulting in a very useful model for experimental data assessment. Additionally, sub-models can be calibrated using TPA to ensure their agreement with experimental data before a predictive model is calibrated. Examples of information obtained from a TPA model are efficiencies, in-cylinder charge temperature, average wall temperatures, spatial wall temperatures, residual gas fraction, heat transfer, BMEP, FMEP, CA50, CA10, and CA90. This model is also computationally inexpensive where, in this work, the total simulation time was about 6 minutes for 34 operating points running on a typical workstation. The main disadvantage of the model is its lack of prediction of engine results without experimental data, however, this is easily circumvented by calibrating a so-called SI Turbulent Flame Combustion Model, which, based on a fully calibrated TPA model, has the ability to predict engine results. Furthermore, the various multipliers available in GT-Power are very useful to circumvent the simplified correlation limitations, however, they can be a tricky option for the unexperienced user, where by over utilizing them one can match experimental data for the wrong reason. Caution and sticking to Gamma Technologies' guidelines are strongly advised when using these multipliers.

In the 3-D CFD models, the chemical kinetics solver SAGE model showed to be a good option for initial simulations when experimental data is not yet available. This is due to the fact that it does not require model constant parameter calibration as in the G-Equation modelling approach. In this work, by virtue of matching CA10 and CA50, engine parameters such as PCP, PCP location, CA90, and gIMEP resulted in values close to mean values and well within the experimental data spread (Figure 8 middle). However, chemical mechanism accuracy affects SAGE results and performance and, therefore, it is usually a more computationally expensive simulation depending on the size of the mechanism used. In this work, average simulation time with SAGE was 29% longer than the G-Equation modelling approach. On the other hand, G-Equation can not only be more computationally efficient but also take advantage of more detailed chemical kinetics for the flame speed lookup table generation and the use of reduced mechanisms in the end gas for knock detection, since flame propagation and chemistry are decoupled. This method allows one to use more accurate/detailed chemistry where it is needed without severely compromising computational efficiency. However, as stated before some level of calibration is necessary for the model parameters, such as the b_1 constant [27], [31] making it a less predictive model. Lastly, G-Equation allows for the calculation of the flame speeds in the domain by solving equation (2) and, since this is an important fuel property, the G-Equation approach was chosen for the analysis of EGAI.

5.2 Natural Gas EGAI Analysis

The models created by this work are intended to aid in the understanding of NG EGAI combustion, i.e. engine parameters and fuel properties that lead to end-gas autoignition, and shine light on possible strategies on to operate a NG engine in a controlled end-gas autoignition (C-EGAI) mode.

An interesting observation is the positive correlation between f-EGAI and KI. As shown in Figure 9, f-EGAI appears to have a linear correlation with KI. The same behavior is captured by the 1-D TPA model where the simulated KI was estimated using Gamma Technologies method [15] which takes into account fuel activation energy, EGR concentration, and equivalence ratio. The implication of this correlation is the possibility to run CFD simulations much more efficiently, since to accurately capture KI in a CFD model one has to run multiple

cycles and set the Mach Courant-Friedrichs-Lewy (CFL) number to be approximately or smaller than 3 [32], [18] in order to properly capture the pressure fluctuations inside the cylinder. If a correlation between KI and f-EGAI exits, then one could use the approach taken in this work, namely single cycle simulation with Mach CFL set to 50, to estimate KI for a given engine from f-EGAI and greatly reduce computational expense.

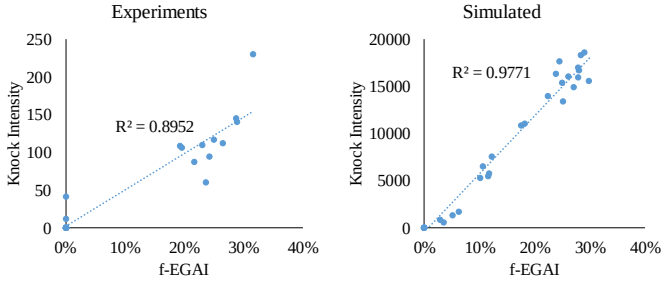

Figure 9: Linear relationship between measured (left) and simulated (right) KI and f-EGAI.

Additionally, Figure 10 shows that there is an opportunity to increase engine efficiency by using C-EGAI. As it can be seen, by increasing f-EGAI, indicated efficiency also increases up to a maximum before falling off. It is also important to highlight that the knocking cases shown in Figure 10 had many parameters varying at the same time, so it should not be considered to directly correlate f-EGAI on indicated efficiency. Even though the correlation for the points in this work are not ideal, our other work have shown promising experimental results [8], [9], [33]. Here again, 1-D TPA model captured well the experimental observations, further validating its accuracy and utility.

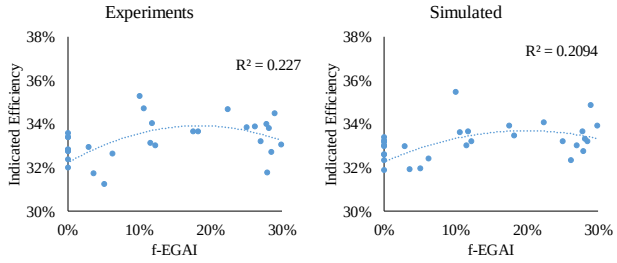

Figure 10: f-EGAI versus Indicated Efficiency measured (left) and estimated using 1-D TPA GT-Power model (right).

Furthermore, additional important observations can be made using the 3-D CFD results. Figure 11 shows the effect of increasing EGR fraction on EGAI. It can be seen that EGAI is reduced with higher EGR rates as a result of the combined effect of lower end-gas temperatures and reduced laminar flame speeds (LFS). Retarding CA50 and lowering CR also shows the same suppressing effect on EGAI due to cooled end-gas temperatures. Figure 12 shows this observation for two different CA50's.

The CFD results not only shed light on the role of LFS and fuel ignition chemistry on EGAI (as seen in Figures 11 and 12), but also highlight the importance of specific heat ratios on EGAI. With faster LFS and longer ignition delays for the same temperature and pressure, the reference MN mixture of H_2/CH_4

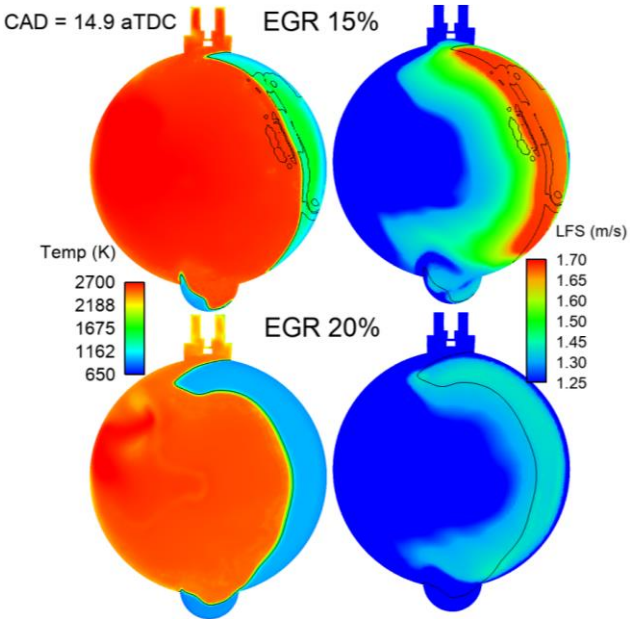

Figure 11: EGR effect on EGAI. EGR has a cooling effect (left) on combustion which suppresses EGAI.

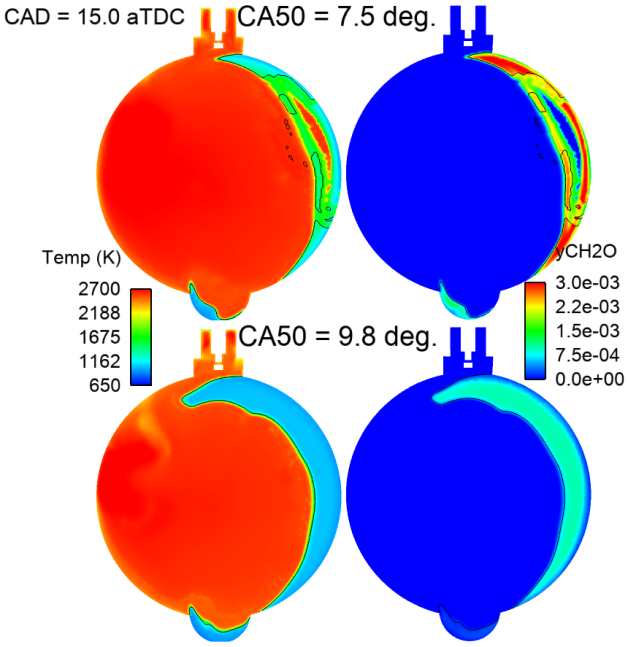

Figure 12: Suppressing effect of retarded CA50 due to lower end-gas temperature (left). Production and consumption of formaldehyde (right) indicating knock occurrence.

should theoretically have a lower propensity to knock than the comparative NG as all of the unburned gas would be consumed before any autoignition could take place. However, its higher specific heats ratio (as a result of the significant H_2 fraction) increases unburned gas temperatures which in turn decreases its ignition delay for the same operating condition, explaining similar observed and simulated auto-ignition timing and KI as its

counterpart NG composition [10]. This is shown in Figures 13 and 14. Table 3 reports the LFS and ignition delays for Pipeline 2 and its MN reference mixture at the same temperature and pressures (60 bar, 900 K) and at peak cylinder pressure (PCP) conditions for each case (Pipeline Day 2: 55.52 bar, 873.9 K; MN Ref.: 56 bar, 889.1 K). It is important to note that the LFS contours show numerical values of LFS for the burned gases and for the unburned gases away from the flame. This is simply an artifact of the post-processing process and it does not affect the calculated LFS during simulation runtime, which take into account the adjacent unburned cells only. The black lines on the contours help visualize flame location.

	60 bar, 900 K		Conditions at PCP	
	LFS	Ign. Delay	LFS	Ign. Delay
Pipeline Day 2	84.4	4.32	80.0	34.55
MN Ref. H_2/CH_4	87.7	5.63	83.3	29.69

Table 3: LFS and Ignition Delay comparison between fuels at the same thermodynamic conditions and those corresponding to the tested peak cylinder pressure (PCP).

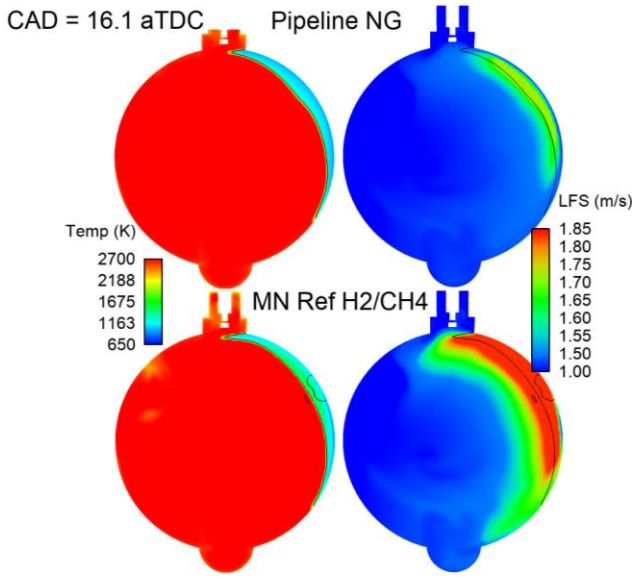

Figure 13: Even with faster LFS and longer ignition delay, the MN reference mixture has similar KI to the Pipeline 2 NG due to increased unburned gas temperature (left).

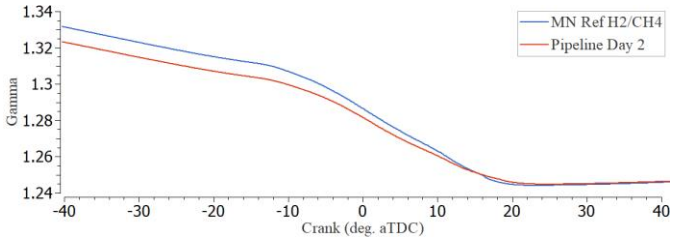

Figure 14: Specific heats ratio of NG 'Pipeline 2' and its MN reference mixture of H_2 and CH_4.

6 CONCLUSIONS

In this study, three computational models of the CFR engine were developed to support the study of EGAI in Spark-Ignited Natural Gas combustion. All of the three models predict with good agreement CFR engine results and aid the investigation of fuel-engine interactions that lead to EGAI.

The GT-Power TPA model showed to be a very useful tool to analyze experimental data and gain insights of various trends. Insights obtained from experimental data and CFD results show that if KI and f-EGAI can be correlated, a single cycle simulation can be sufficient to predict KI in a given engine at significantly reduced computational expense. This improvement, however, is constrained by having an accurate 1-D model to predict initial and boundary conditions and by accurately predicting f-EGAI. The average simulation time for all CFD simulations presented in this work was 17-18 hours on 40 cores.

Additionally to the identification of each model's advantages and disadvantages, the following was observed:

1. There is a linear relationship between f-EGAI with KI (Figure 9);
2. There is an opportunity to increase SI NG engine efficiency by having controlled levels of f-EGAI (Figure 10);
3. And the similar knocking behavior of NG fuel and its reference CH_4/H_2 mixtures can be understood by understanding the interactions between laminar flame speeds, ignition delays, and the thermodynamic conditions of the end gas;

Future work is still necessary to address uncertainties such as the influence of NOx chemistry on EGAI and how the inclusion of NOx chemistry would affect the prediction of f-EGAI using the computational models. Furthermore, a predictive 1-D model combined with real-time control algorithms would be helpful for the study and optimization of C-EGAI operation.

ACKNOWLEDGEMENTS

This research is funded by the U.S. Department of Energy under grant number DE-EE0008331. The authors also would like to thank Convergent Science for providing CONVERGE CFD licenses for this study.

REFERENCES

[1] Reitz, R. D., 2013, "Directions in internal combustion engine research," Combustion and Flame, 1(160), pp. 1-8.
[2] Kalghatgi, G. T., 2014, "The outlook for fuels for internal combustion engines," International Journal of Engine Research, 15(4), pp. 383-398.
[3] Kalghatgi, G., 2015, "Developments in internal combustion engines and implications for combustion science and future transport fuels," Proceedings of the Combustion Institute, 35(1), pp. 101-115.
[4] Mitchell, R. H., and Olsen, D. B., 2018, "Extending Substitution Limits of a Diesel–Natural Gas Dual Fuel Engine," Journal of Energy Resources Technology, 140(5), p. 052202.

[5] Das, A., and Watson, H., 1997, "Development of a natural gas spark ignition engine for optimum performance," Proceedings of the Institution of Mechanical Engineers, Part D: Journal of Automobile Engineering, 211(5), pp. 361-378.
[6] Heywood, J., "1988, Internal Combustion Engine Fundamentals, McGraw-Hill, New York."
[7] Standard, A., 2004, "Standard test method for research octane number of spark-ignition engine fuel," D2699, Rev. December.
[8] Bayliff, S., Windom, B., Marchese, A., Hampson, G., Carlson, J., Chiera, D., and Olsen, D., 2020, "CONTROLLED END GAS AUTO IGNITION WITH EXHAUST GAS RECIRCULATION ON A STOICHIOMETRIC, SPARK IGNITED, NATURAL GAS ENGINE," Proceedings of the ASME 2020 Internal Combustion Fall Technical Conference.
[9] Bayliff, S., 2020, "EVALUATION OF CONTROLLED END GAS AUTO IGNITION WITH EXHAUST GAS RECIRCULATION IN A STOICHIOMETRIC, SPARK IGNITED, NATURAL GAS ENGINE," Master of Science, Colorado State University, Colorado State University.
[10] Bestel, D., Bayliff, S., Marchese, A., Olsen, D., Windom, B., and Xu, H., 2020, "Investigation of the End-Gas Autoignition Process in Natural Gas Engines and Evaluation of the Methane Number Index," Proceedings of the Combustion Institute (submitted).
[11] Waukesha, C., 2003, "F-1 & F-2 Research method (F-1), Motor method (F-2), Octane rating units, Operation & maintenance," Dresser Inc.
[12] Wise, D. M., Olsen, D. B., and Kim, M., "Characterization of methane number for producer gas blends," Proc. ASME 2013 Internal Combustion Engine Division Fall Technical Conference, American Society of Mechanical Engineers Digital Collection.
[13] Choi, S., Kolodziej, C. P., Hoth, A., and Wallner, T., 2018, "Development and Validation of a Three Pressure Analysis (TPA) GT-Power Model of the CFR F1/F2 Engine for Estimating Cylinder Conditions," No. 0148-7191, SAE Technical Paper.
[14] Pal, P., Kolodziej, C., Choi, S., Som, S., Broatch, A., Gomez-Soriano, J., Wu, Y., Lu, T., and See, Y. C., 2018, "Development of a virtual cfr engine model for knocking combustion analysis," SAE International Journal of Engines, 11(6), pp. 1069-1082.
[15] Technologies, G., 2018, "GT-Power 2018."
[16] Morganti, K. J., 2013, "A study of the knock limits of liquefied petroleum gas (LPG) in spark-ignition engines."
[17] Woschni, G., 1967, "A universally applicable equation for the instantaneous heat transfer coefficient in the internal combustion engine," No. 0148-7191, SAE Technical paper.
[18] Sciences, C., 2019, "CONVERGE CFD."
[19] Givler, S. D., Raju, M., Pomraning, E., Senecal, P., Salman, N., and Reese, R., 2013, "Gasoline combustion modeling of direct and port-fuel injected engines using a reduced chemical mechanism," No. 0148-7191, SAE Technical Paper.
[20] Pomraning, E., Richards, K., and Senecal, P., 2014, "Modeling turbulent combustion using a RANS model, detailed chemistry, and adaptive mesh refinement," No. 0148-7191, SAE Technical Paper.
[21] Scarcelli, R., Richards, K., Pomraning, E., Senecal, P., Wallner, T., and Sevik, J., 2016, "Cycle-to-cycle variations in multi-cycle engine RANS simulations," No. 0148-7191, SAE Technical Paper.
[22] Amsden, A., O'Rourke, P., and Butler, T., 1989, "A Computer Program for Chemically Reactive Flows with Sprays, Los Alamos Laboratory," Report LA-11560-MS.
[23] Senecal, P., Pomraning, E., Richards, K., Briggs, T., Choi, C., McDavid, R., and Patterson, M., 2003, "Multi-dimensional modeling of direct-injection diesel spray liquid length and flame lift-off length using CFD and parallel detailed chemistry," SAE transactions, pp. 1331-1351.
[24] Zhou, C.-W., Li, Y., Burke, U., Banyon, C., Somers, K. P., Ding, S., Khan, S., Hargis, J. W., Sikes, T., and Mathieu, O., 2018, "An experimental and chemical kinetic modeling study of 1, 3-butadiene combustion: Ignition delay time and laminar flame speed measurements," Combustion and Flame, 197, pp. 423-438.
[25] Mohr, J., 2020, "The Effect of Fuel Reactivity and Exhaust Gas Recirculation on Knock Propensity of Natural Gas," Master of Science, Colorado State University, Colorado State University.
[26] Mohr, J., Windom, B., Olsen, D., and Marchese, A., 2020, "HOMOGENEOUS IGNITION DELAY, FLAME PROPAGATION RATE AND END-GAS AUTOIGNITION FRACTION MEASUREMENTS OF NATURAL GAS AND EXHAUST GAS RECIRCULATION BLENDS IN A RAPID COMPRESSION MACHINE," Proceedings of the ASME 2020 Internal Combustion Engine Division Fall Technical Conference (submitted).
[27] Peters, N., 2000, "Turbulent combustion. Cambridge, UK: Cambridge University Press."
[28] Ewald, J., and Peters, N., "A level set based flamelet model for the prediction of combustion in spark ignition engines," Proc. 15th International Multidimensional Engine Modeling User's Group Meeting, Detroit, MI.
[29] Morganti, K. J., Brear, M. J., da Silva, G., Yang, Y., and Dryer, F. L., 2015, "The autoignition of Liquefied Petroleum Gas (LPG) in spark-ignition engines," Proceedings of the Combustion Institute, 35(3), pp. 2933-2940.
[30] Foong, T. M., Brear, M. J., Morganti, K. J., da Silva, G., Yang, Y., and Dryer, F. L., 2017, "Modeling end-gas autoignition of ethanol/gasoline surrogate blends in the cooperative fuel research engine," Energy & Fuels, 31(3), pp. 2378-2389.
[31] Abdel-Gayed, R. G., and Bradley, D., 1981, "A two-eddy theory of premixed turbulent flame propagation," Philosophical transactions of the royal society of London. Series A, Mathematical and physical sciences, 301(1457), pp. 1-25.
[32] Yue, Z., Edwards, K. D., Sluders, C. S., and Som, S., 2019, "Prediction of Cyclic Variability and Knock-Limited Spark Advance in a Spark-Ignition Engine," Journal of Energy Resources Technology, 141(10).
[33] Hampson, G. J., "High Efficiency Natural Gas Engine Combustion Using Controlled Auto-Ignition," Proc. ASME 2019 Internal Combustion Engine Division Fall Technical

Conference, American Society of Mechanical Engineers Digital Collection.

